The Lateral Dynamics of a Nonsmooth Railway Wheelset Model

Zhang, Tingting; True, Hans; Dai, Huanyun

Published in:
International Journal of Bifurcation and Chaos

Link to article, DOI:
10.1142/S0218127418500955

Publication date:
2018

Document Version
Peer reviewed version

International Journal of Bifurcation and Chaos, Vol. 28, No. 8 (2018) 1850095 (15 pages)

DOI: 10.1142/S0218127418500955

The Lateral Dynamics of a Nonsmooth Railway Wheelset Model

Tingting Zhang*,†,‡, Hans True*,†,§ and Huanyun Dai*,¶
*State Key Laboratory of Traction Power,
Southwest Jiaotong University, Chengdu,
Sichuan 610031, P. R. China
†DTU Compute, The Technical University of Denmark,
DK-2800 Kgs.Lyngby, Denmark
‡zhangt@student.dtu.dk
§htru@dtu.dk
¶daihuanyun@163.com

Received July 26, 2017; Revised May 22, 2018

In this paper, we investigate the lateral dynamics of a railway wheelset suspended under a moving car with linear springs and dry friction dampers. Both theoretical and numerical methods are used to complement each other. The car runs on an ideal, straight and perfect track with a constant speed. A nonlinear relation between the creepages and the creep forces is used in this paper. The nonsmoothness of this model is due to the dry friction dampers. The speed is selected as the bifurcation parameter. The one-dimensional bifurcation diagram, which gives a general view of the dynamics of the system, is presented. Both symmetric and asymmetric periodic motions, quasi-periodic motions and chaotic motions are found. In addition to bifurcations that can exist in both smooth and nonsmooth systems, a kind of sliding bifurcations that are unique to nonsmooth systems is found. Bifurcation diagrams, phase portraits, Poincaré sections and Lyapunov exponents are presented to ensure that no contradictory results are given. The influence of the conicity of the wheel tread on the Hopf bifurcation type is examined.

Keywords: Railway wheelset; nonlinearity; nonsmoothness; bifurcations; chaos.

1. Introduction

Railway vehicle dynamics as an interesting topic in railway engineering has been investigated by researchers for more than a century. The fundamental railway guidance system consists of a flanged rigid wheelset and two rigid rails. When the wheelset runs above a certain critical speed it may oscillate laterally combined with a yaw motion that is known as the hunting motion of the wheelset. Based on the kinematic instability the basic analysis of the hunting motion was done by Klingel [1883]. Since no dynamical forces were considered in his paper, he could not explain the difference between the theory and the experimental results. Carter [1916] first included the dynamical forces in the wheelset stability problem. Later, for the first time, Huilgol [1978] introduced the bifurcation analysis from nonlinear dynamics into the railway vehicle dynamical problems, which initiated a new trend of investigations among the railway engineers around the world. Possel *et al.* [1960] presented a best stability analysis of a two-axle railway vehicle in 1950,

‡Author for correspondence

and won a prize provided by the Office for Research and Experiments of the Union of International Railways.

With the spread and development of bifurcation theory, many dynamical railway applications are possible. True and Kaas-Petersen [1983] found that the bifurcation to periodic motion is subcritical and the critical speed must be found by an investigation of the existence of multiple attractors. They used Kaas-Petersen's program 'PATH' [Kaas-Petersen, 1986b] for the investigations of both the stable and unstable stationary and periodic solutions. Kaas-Petersen [1986a] used this program for the investigation of the dynamical motion of a railway bogie model and discovered chaos in this model. Knudsen *et al.* [1992] discovered both symmetric and asymmetric oscillations and chaos in a model of a rolling railway wheelset that were used to explain a lopsided wear of the wheelset. Knudsen *et al.* [1994] extended the investigations in another paper [Jensen & True, 1997] and discussed the different transitions to chaos. Gao *et al.* [2012], Gao *et al.* [2013], Gao *et al.* [2015] put forward the "resultant bifurcation diagram" method to investigate the symmetric/asymmetric periodic and chaotic motions in the symmetric railway vehicle models. They also found that symmetry breaking bifurcations and symmetry restoring bifurcations happened repeatedly in the symmetric railway vehicle models, and finally chaotic attractors appeared through a series of period doubling bifurcations or quasi-periodic motions.

The nonsmoothness of the former mentioned researches was mainly from the flanged wheels. In real life, however, the nonsmoothness often exists in the form of impact, sliding, switching and other discrete state transitions. Xia [2002] investigated the dynamics of a nonsmooth three-piece-freight truck in his PhD thesis. Because of the dry friction, sticking and sliding motions exist in this model, which leads to a discontinuity in the behavior of the dynamical system, and leads to a collapse of the state space. Hoffmann and Petersen [2003] studied the dynamics of a Hbbills 311 freight wagon with dry friction and impact. With the development of the nonsmooth dynamical theory in recent years, a lot of research has appeared. Andronov *et al.* [1965] investigated nonsmooth equilibrium bifurcations. Feigin [1994] introduced C-bifurcations into the piecewise-smooth dynamical systems. Filippov [1988] studied sliding motions of nonsmooth dynamical systems. With regard to the concepts, definitions and methods about the analysis of nonsmooth bifurcations we refer readers to the books by di Bernardo *et al.* [2008] and Simpson [2010]. True and Asmund [2002] first unveiled the dynamics of a railway wheelset system containing a coupling between a dry friction damper and the basic nonlinearity (the wheel/rail contact forces), in railway dynamics with regard to railway vehicle nonsmooth dynamics. True and Thomsen [2005] and True *et al.* [2013] tested several integrators (both explicit and implicit) to demonstrate how the numerical railway vehicle nonsmooth dynamical problems are solved, and how reliable dynamic results are obtained. They also compared the performances of different integrators with respect to the accuracy and the time consumed.

In this paper, the bifurcation behavior and chaotic motions of a railway wheelset with dry friction dampers are examined. This model, without dry friction dampers, was studied by Knudsen *et al.* [1992], Silvsgaard and True [1994]. The running speed V is chosen as the control parameter with all other parameters constant. Both smooth bifurcations, that can exist in smooth as well as nonsmooth dynamic systems, and nonsmooth bifurcations, that only exist in nonsmooth dynamic systems, are found in this simple model. In the low speed range both subcritical Hopf bifurcation and a saddle-node bifurcation, that are common in the models without dry friction dampers, are found. The crossing-sliding bifurcation, which is special for nonsmooth dynamical systems, is also found. Furthermore, a Neimark–Sacker bifurcation is found at a higher speed than the Hopf bifurcation point. Different transitions among periodic windows, quasi-periodic motions and chaotic attractors are discussed in detail in different speed ranges. Finally, the influence of the conicity of the wheel tread on the Hopf bifurcation forms is investigated.

2. The Mathematical Model

A schematic diagram of a railway wheelset model with lateral dry friction dampers is shown in Fig. 1. The coordinate system used for the description of the mechanical model is also shown in Fig. 1. The wheelset is suspended under a moving car running on an ideal, straight and perfect track with a constant speed. Both the wheels and the rails are rigid bodies. It is assumed that the wheels and the rails

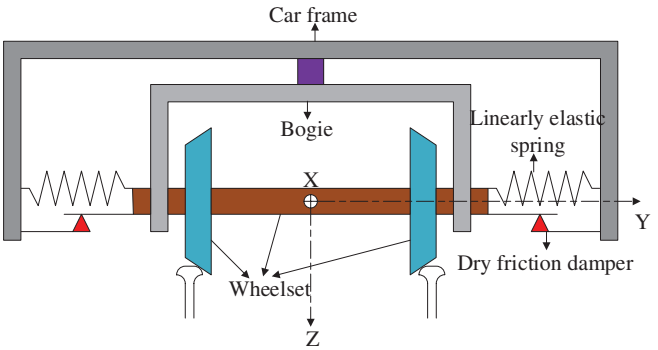

Fig. 1. Schematic diagram of a nonsmooth wheelset model.

remain at one-point contact. The wheel profile is conical. The rail surface is an arc of a circle. The wheelset can move laterally in the bogie frame, which is connected to the car through a frictionless vertical pivot, linear springs and dry friction dampers. The transfer of the weight of the car body and the bogie frame is included but not specified in the model. To consider the worst case of the dynamical behavior of this model, no yaw stiffness is considered here. To emphasize the influence of the dry friction dampers on the bifurcations and chaos, the nonsmoothness caused by the flange contact force is neglected in this paper.

The wheelset model has two degrees of freedom, which are the lateral and yaw motion of the wheelset model. The nonlinearities in this model mainly stem from the nonlinear relation between the creepages and the creep forces and the dry friction dampers. The lateral displacement and the yaw angle are denoted as y_w and ψ respectively. According to the linear kinematic relation between the wheel and the rail, the longitudinal and lateral creepage can be expressed as:

$$\begin{cases} \xi_x = \dfrac{a\dot{\psi}}{V} + \dfrac{\lambda y_w}{r_0}, \\ \xi_y = \dfrac{\dot{y}_w}{V} - \psi, \end{cases} \tag{1}$$

where a dot above the variable means differentiation with respect to time, and the meaning and value of other symbols that can be found in [Knudsen *et al.*, 1992; True & Asmund, 2002], are listed in Table 1.

According to the creepage-creep force relation by Vermeulen and Johnson [1964], we can get the expressions for the resultant creep force F_R:

$$F_R = \mu_t N \begin{cases} u - \dfrac{1}{3}u^2 + \dfrac{1}{27}u^3, & u < 3, \\ 1, & u \geq 3, \end{cases} \tag{2}$$

with the longitudinal component F_x and the lateral component F_y as:

$$\begin{cases} F_x = \dfrac{\xi_x F_R}{\Phi \xi_R}, \\ F_y = \dfrac{\xi_y F_R}{\Psi \xi_R}, \end{cases} \tag{3}$$

where $\xi_R = \sqrt{(\xi_x/\Phi)^2 + (\xi_y/\Psi)^2}$ is the resultant creepage, and $u = (G\pi a_e b_e/\mu_t N) = C\xi_R/\mu_t N$.

As for the dry friction dampers, the dry friction model from the paper [True & Asmund, 2002], that is convenient for numerical realization without losing the essential characteristics, is selected. The expression for the dry friction dampers in this model is:

$$F_\mu = F_d \operatorname{sech}(\alpha \dot{y}_w) + F_s(1 - \operatorname{sech}(\alpha \dot{y}_w)). \tag{4}$$

Therefore, the mathematical model of the wheelset can be formulated as:

$$\begin{cases} m\ddot{y}_w + 2F_y - 2K_s y_w - \operatorname{sign}(\dot{y}_w)F_\mu = 0, \\ I\ddot{\psi} + 2aF_x = 0. \end{cases} \tag{5}$$

Table 1. Wheelset parameters.

Parameter	Comment	Value
m	Mass of the wheelset	1022 kg
I	Yaw moment of wheelset	678 kg · m^2
a	Half the distance between the contact points	0.75 m
C	Constant related to the resultant creep force	6.5630 MN
K_s	Lateral spring stiffness	1 MN · m^{-1}
Ψ	Lateral wheel-rail contact parameter	0.54219
Φ	Longitudinal wheel-rail contact parameter	0.60252
r_0	Centered wheel rolling radius	0.4572 m
λ	Conicity	0.15
μ_t	Coefficient of adhesion	0.15
$\mu_t N$	N is the vertical force between wheel and rail	10 kN
α	A scaling factor	50 m/s
F_d	Kinetic friction force of dry friction dampers	1000 N
F_s	Static friction force of dry friction dampers	1200 N
V	Speed of the wheelset	—

We make a change of variables, $[x_1, x_2, x_3, x_4] = [y_w, \dot{y}_w, \psi, \dot{\psi}]$, to obtain the following four first-order autonomous piecewise-smooth differential equations:

$$\begin{cases} \dot{x}_1 = x_2, \\ \dot{x}_2 = -\dfrac{2F_y}{m} + \dfrac{2K_s x_1}{m} + \operatorname{sign}(x_2)\dfrac{F_\mu}{m}, \\ \dot{x}_3 = x_4, \\ \dot{x}_4 = -\dfrac{2aF_x}{I}. \end{cases} \tag{6}$$

3. The Method of Investigation

The dynamical system of the wheelset model can be viewed as an initial value problem of a set of first-order autonomous piecewise-smooth differential equations. Here we select the speed of the wheelset as the control parameter with other parameters constant. Due to the nonlinearities and the nonsmoothnesses in this model, it is impossible to investigate the bifurcations and chaos in a purely analytic way. Since the system is of low dimension, we can combine the analytic method with the numerical analysis.

The pseudo-arclength continuation method and Newton's iteration are used to follow the stationary solutions. The bifurcation of periodic orbits from the stationary solutions, that is known as a Hopf bifurcation, is located according to the method proposed by Zou *et al.* [2006], and the Hopf bifurcation type is determined from the first Lyapunov coefficient [Kuznetsov, 2004]. Because of the dry friction dampers in the system, a special sliding bifurcation is determined based on the theory of sliding bifurcations in Filippov systems [di Bernardo *et al.*, 2008].

For the numerical integrations we apply the standard ode45 function in MATLAB with a variable step size. According to a trial-and-error approach both the absolute and relative error are set to 10^{-7} to make a compromise between the accuracy of the solutions and the time consumption. The bifurcation diagram is constructed through an increase and decrease process of the speed based on a Poincaré map. Here the Poincaré map is defined by $\prod = \{(x, V) \in R^4 \times R^+ \,|\, x_1 \geq 0, x_2 = 0\}$.

In order to investigate the quasi-periodic and chaotic behaviors of the wheelset model we continue the integration after the transients have died out. Phase portraits, Poincaré sections and Lyapunov exponents are computed to distinguish the quasi-periodic motions from the chaotic motions. We emphasize here that different methods are used so that no contradictory results are given. The Lyapunov exponents, which measure the mean convergence or divergence of the nearby trajectories in the phase space, are the most efficient indicators to determine if the motion of the system is quasi-periodic or chaotic. In this paper, we use Wolf's method [Wolf *et al.*, 1985] to calculate the Lyapunov exponents of the wheelset system. We choose a time step of 0.5 s for the Gram–Schmidt renormalization procedure. Refer to [Wolf *et al.*, 1985] for the details of the numerical calculation of the Lyapunov exponents of dynamic systems from time series.

4. Some Results

The full bifurcation diagram in the speed range between 35 m/s and 65 m/s was computed and shown in Fig. 2 according to the numerical methods mentioned in the last section. Compared with the wheelset without dry friction dampers [Knudsen *et al.*, 1992], a set of stationary points takes the place of the globally stable trivial solutions. The qualitative behavior of the system at $V = 35$ m/s is shown in Fig. 3 from which we can see that in the stationary state the lateral displacement is zero, but the yaw angle is different from zero. From the point of view of physics, because of the existence of the friction damper in the model, the wheelset can run without hunting motions under a low running speed

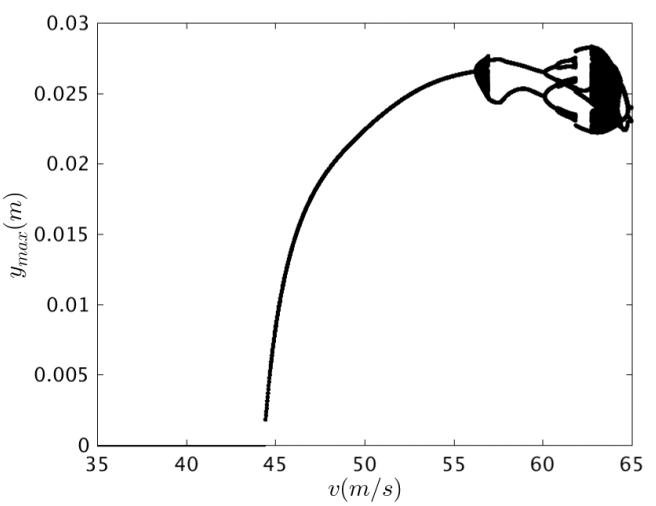

Fig. 2. Bifurcation diagram for the wheelset model. (Only stable solutions are shown.)

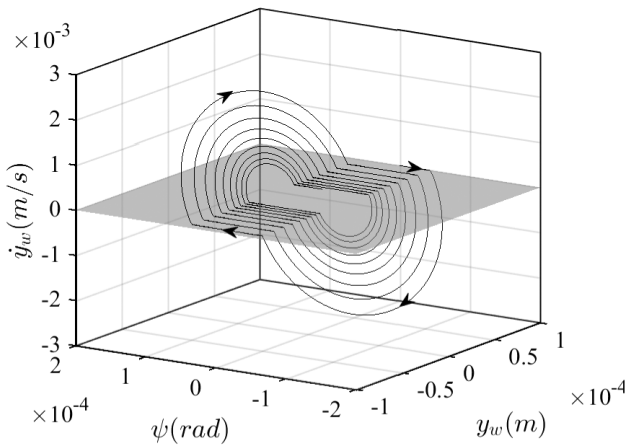

Fig. 3. Qualitative behavior of the system at $V = 35\,\mathrm{m/s}$.

even if its yaw angle with respect to the track center line is different from zero.

Assume that the linearized system of both sides has a pair of complex conjugate eigenvalues $\alpha^{\pm}(V) \pm i\omega^{\pm}(V)$, where $+$ and $-$ indicate the right and the left sides respectively, and $i^2 = -1$. Let

$$B(V) = \frac{\alpha^{+}(V)}{\omega^{+}(V)} + \frac{\alpha^{-}(V)}{\omega^{-}(V)}. \tag{7}$$

As the speed is increased, a subcritical Hopf bifurcation [Eva, 1992; True, 1993] will be reached at $V = 44.4571\,\mathrm{m/s}$ which is confirmed by Fig. 4 with $B(V) = 0$ and a positive first Lyapunov coefficient $l_1(0) = 1.3738 \times 10^{10}$. An unstable limit cycle bifurcates to the left side of the Hopf bifurcation point, and it continues until $V = 44.4450\,\mathrm{m/s}$ where the unstable limit cycle regains its stability through a saddle-node bifurcation. From this point and increasing the speed with a small step, a crossing-sliding bifurcation, where the two sliding segments vanish, will be reached at $V = 44.5080\,\mathrm{m/s}$. At this point

$$[x_1, x_2, x_3, x_4] = [0.0026\,\mathrm{m}, 0.0000\,\mathrm{m/s}, 1.8017 \times 10^{-4}\,\mathrm{rad}, -0.0509\,\mathrm{rad/s}],$$

which satisfies all the conditions from [di Bernardo *et al.*, 2008] for a crossing-sliding bifurcation to happen. Orbits of the system before and after the crossing-sliding bifurcation are shown in Fig. 5. To give a better view of the transition at the crossing-sliding bifurcation point, an enlargement of the 2D phase portraits in Fig. 5 is shown in Fig. 6. From Fig. 2, we can see that the system undergoes a periodic motion in a large speed range. A variety of bifurcation phenomena happen in the speed range 56–65 m/s. In the following, the bifurcation analysis in four important speed ranges is elaborated, and transitions between different bifurcations are discussed.

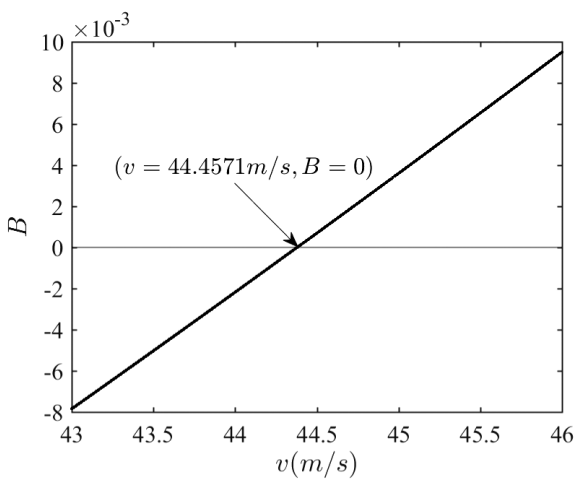

Fig. 4. Detection of Hopf bifurcation point.

4.1. *Speed range 56.2–57 m/s*

A blow-up of the bifurcation diagram in the speed range 56.2–57 m/s is shown in Fig. 7. The transitions in this speed range are of interest because of the sequences of bifurcations in this narrow speed interval, that finally lead to asymmetrical periodic orbits through a crisis. The wheelset undergoes quasi-periodic and periodic motions alternatively during this speed range. The first bifurcation happens around $V = 56.2380\,\mathrm{m/s}$ where the stable limit cycle loses its stability, and an invariant two-dimensional torus appears through a Neimark–Sacker bifurcation. This is illustrated in Fig. 8 where the Poincaré maps were plotted under two different speeds before and after the Neimark–Sacker bifurcation respectively. The Poincaré map is constructed after the transients have died out. It is seen that a point in the Poincaré map converts into a closed curve, which indicates the existence of a biperiodic oscillation.

From Fig. 7 we can see there are six periodic windows during this speed range. Here we only choose the first periodic window to give a detailed analysis of the transitions near this periodic window. A refined bifurcation diagram near this periodic window is shown in Fig. 9. The most noticeable phenomenon is the period-20 window around $V = 56.2843\,\mathrm{m/s}$. The Poincaré map under

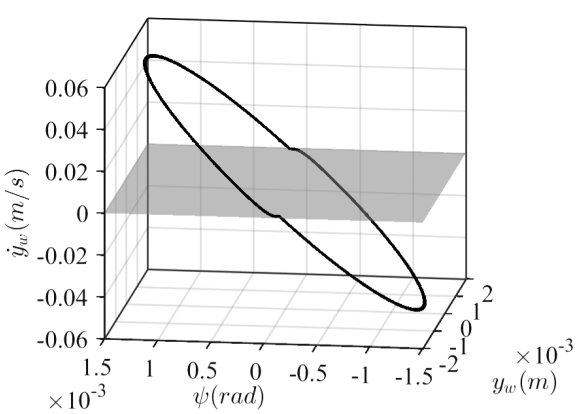

(a) $v = 44.45$ m/s

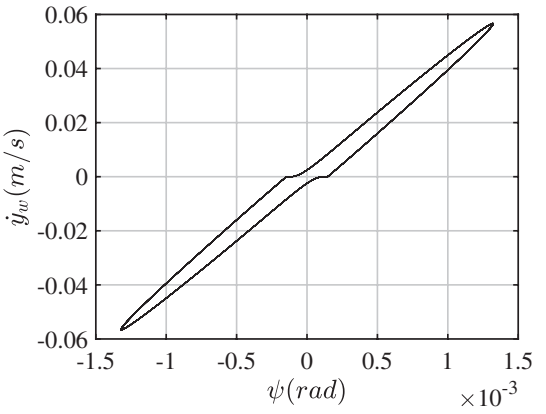

(b) $v = 44.45$ m/s

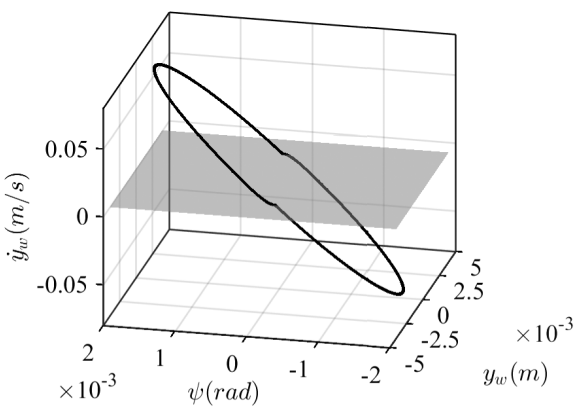

(c) $v = 44.51$ m/s

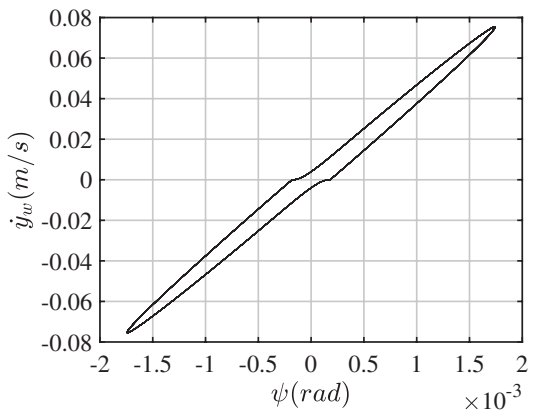

(d) $v = 44.51$ m/s

Fig. 5. Orbits before and after the crossing-sliding bifurcation.

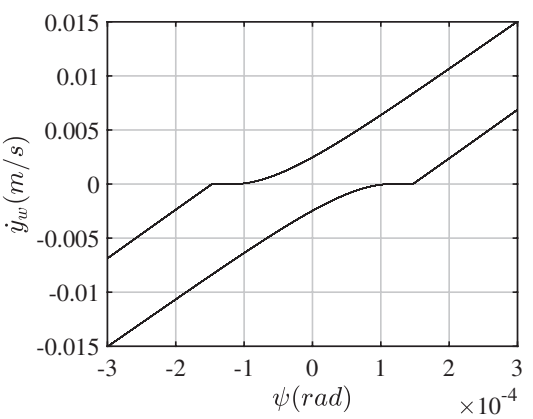

(a) $v = 44.45$ m/s

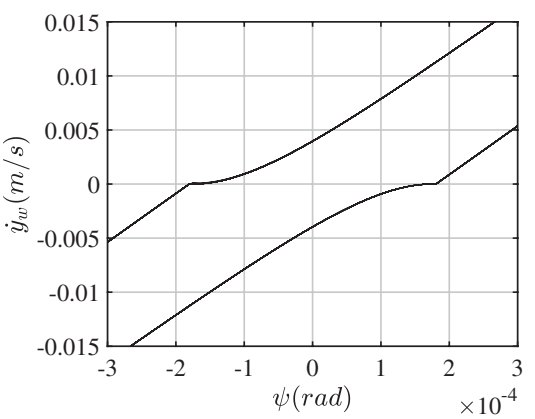

(b) $v = 44.51$ m/s

Fig. 6. Enlargement of 2D phase portraits in Fig. 5.

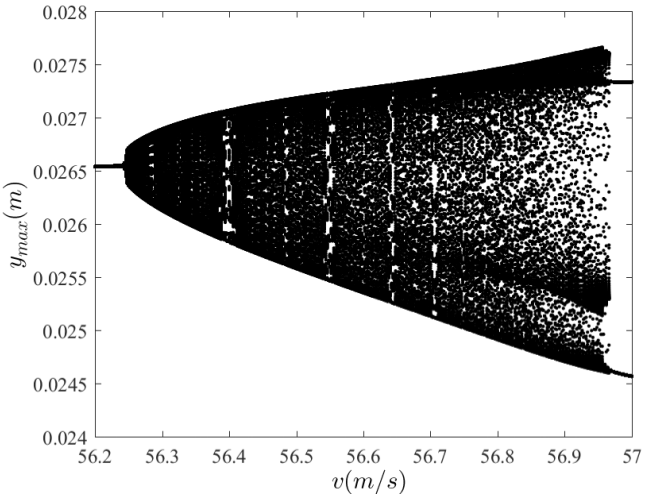

Fig. 7. A blow-up bifurcation diagram in the range 56.2–57 m/s.

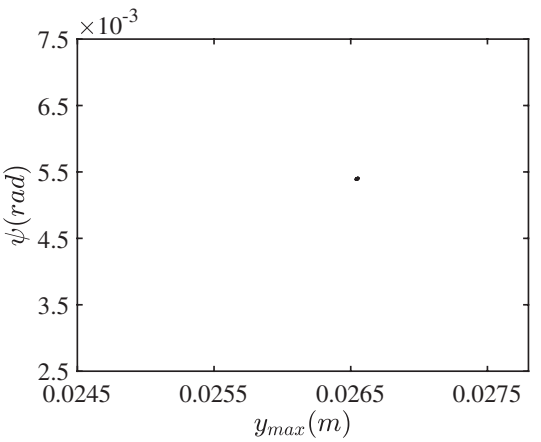

(a) $v = 56.20$ m/s

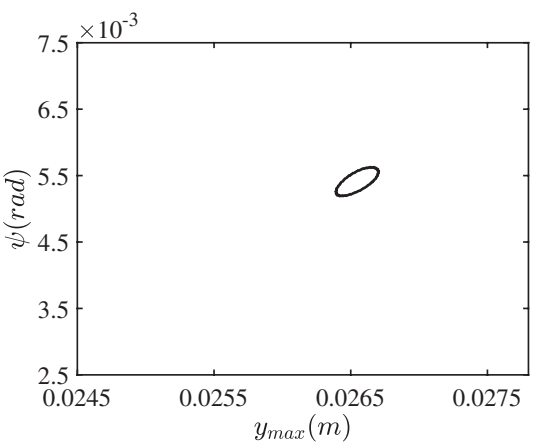

(b) $v = 56.245$ m/s

Fig. 8. Poincaré maps near the Neimark–Sacker bifurcation point.

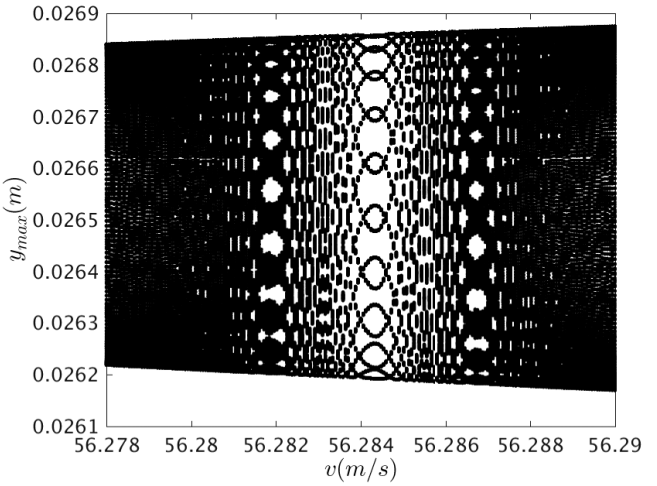

Fig. 9. A refined bifurcation diagram near the first periodic window.

this speed is shown in Fig. 10, which consists of 20 points on a closed curve. The numbers in the figure indicate the sequence of the points appearing on the Poincaré map. On both sides biperiodic solutions will be found, which are confirmed by the discrete arcs on the Poincaré maps. The transitions around the other five periodic windows are similar to this one, which will not be analyzed in detail in this paper.

As the speed increases further, the system enters into chaos through a torus breakdown in the speed range 56.80–56.90 m/s. Comparing the Poincaré maps in Fig. 12, it can be seen that foldings are displayed at the speed of $V = 56.90$ m/s, which are typical features of chaos. The largest two Lyapunov exponents of the system shown in Fig. 12 indicate that chaos occurs at the speed of

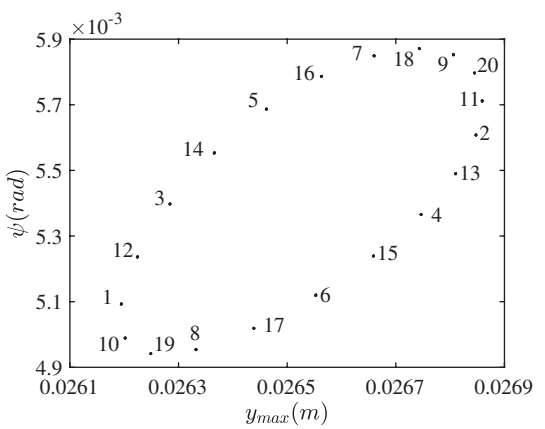

Fig. 10. Poincaré map at $V = 56.2843$ m/s.

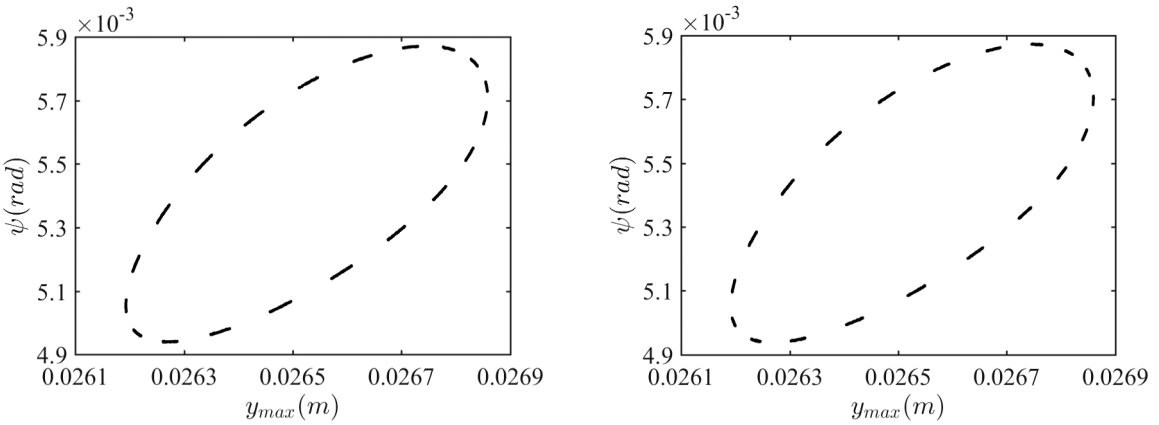

(a) $v = 56.2841$ m/s (b) $v = 56.2845$ m/s

Fig. 11. Poincaré maps on both sides of the periodic window.

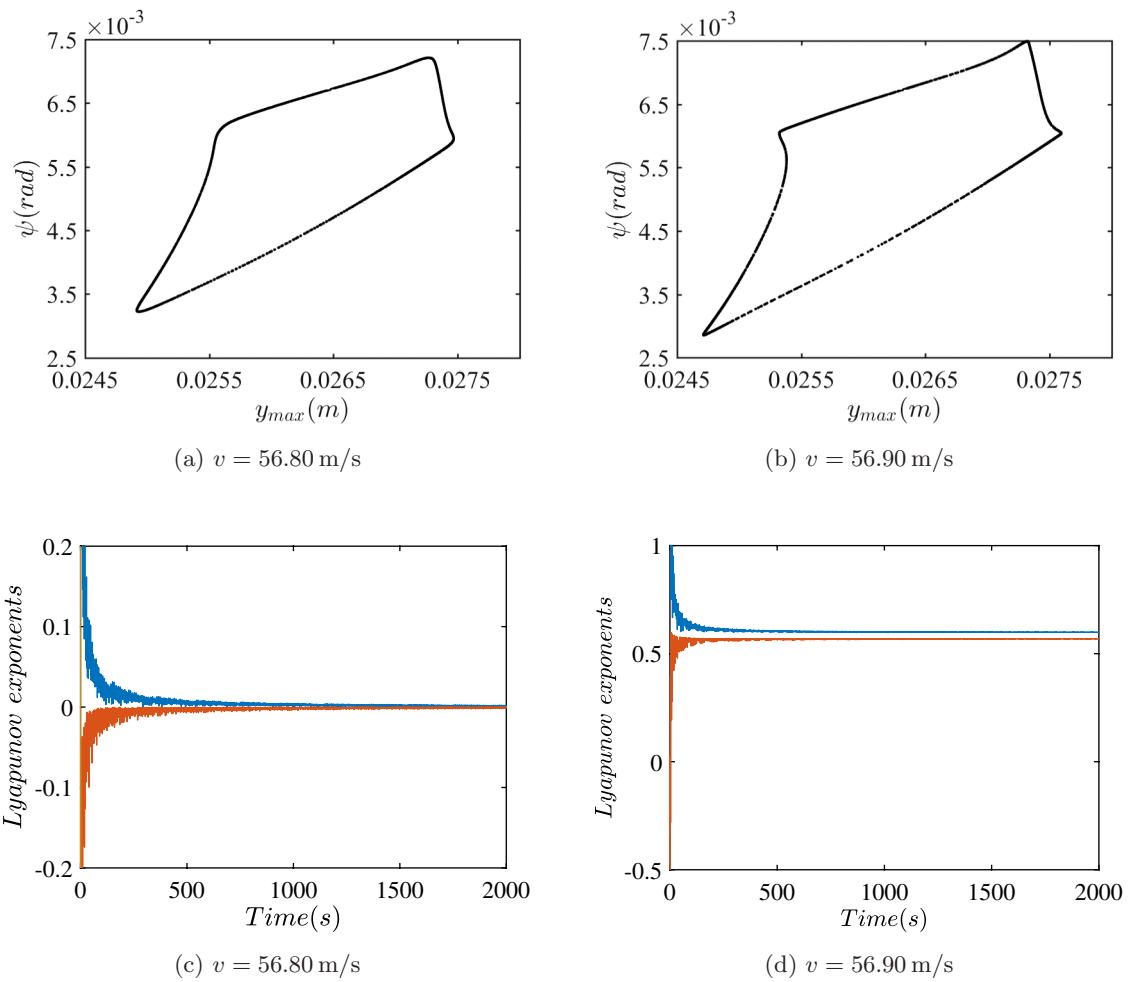

(a) $v = 56.80$ m/s (b) $v = 56.90$ m/s

(c) $v = 56.80$ m/s (d) $v = 56.90$ m/s

Fig. 12. (a) and (b) Poincaré maps and (c) and (d) the two largest Lyapunov exponents.

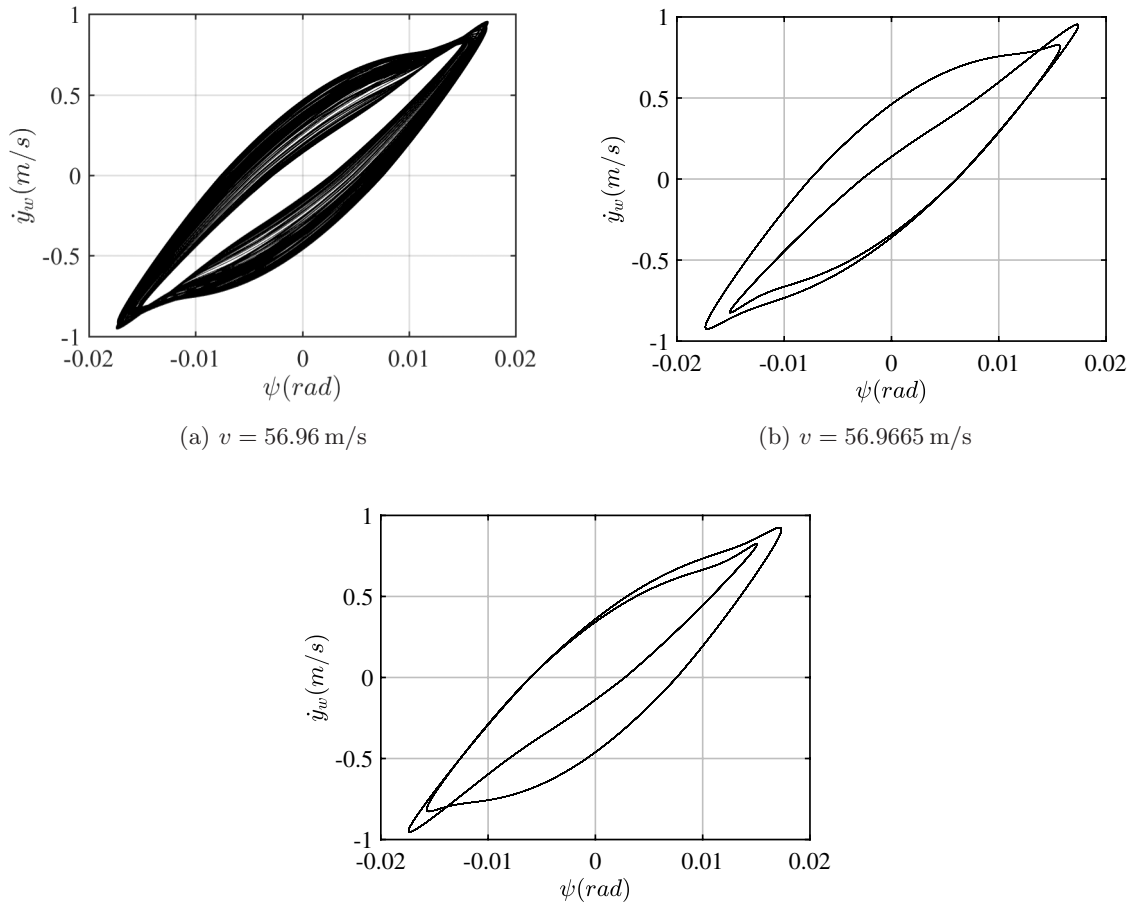

(a) $v = 56.96\,\text{m/s}$

(b) $v = 56.9665\,\text{m/s}$

(c) $v = 56.9665\,\text{m/s}$

Fig. 13. Phase portraits of the model near the crisis.

$V = 56.90\,\text{m/s}$. At around $V = 56.9665\,\text{m/s}$ two asymmetric periodic solutions bifurcate from the chaos through a crisis which is confirmed by the phase portraits of the model near the crisis shown in Fig. 13, where the initial conditions for Figs. 13(b) and 13(c) are

$$[x_1, x_2, x_3, x_4] = [0.0179\,\text{m}, -0.5681\,\text{m/s}, -0.0059\,\text{rad}, -0.5144\,\text{rad/s}]$$

and

$$[x_1, x_2, x_3, x_4] = [-0.0179\,\text{m}, 0.5681\,\text{m/s}, 0.0059\,\text{rad}, 0.5144\,\text{rad/s}]$$

respectively. It can be seen that Fig. 13(c) is a reflection of Fig. 13(b) around the axis ψ(rad) followed by a reflection around the axis $\dot{y}_w$(m/s).

4.2. *Speed range 59.5–61.5 m/s*

From Fig. 2 we can see that the asymmetrical periodic solutions exist in a broad speed range. In this section, we give a detailed bifurcation analysis in the speed range 59.5–61.5 m/s. A blow-up bifurcation diagram in this speed range is shown in Fig. 14. The transitions in this speed range are simple, where the asymmetrical periodic solutions go through period doublings. Therefore, four asymmetrical periodic solutions are created. The asymmetrical periodic solutions undergo a complete period doubling cascade to chaos, which will be explained in the next section. A variety of the characteristic periodic windows are shown in Fig. 15. It can be seen that the two period doubling cascades cross with the others four times (here we only show the first one at around $V = 60.77\,\text{m/s}$. Except for the left-top dot the other three dots consist of two points each.

4.3. *Speed range 61.6–62.2 m/s*

With the increase of the speed the system enters into chaos through a period doubling cascade. A refined bifurcation diagram in speed range 61.6–62.2 m/s is shown in Fig. 16 (constructed with an

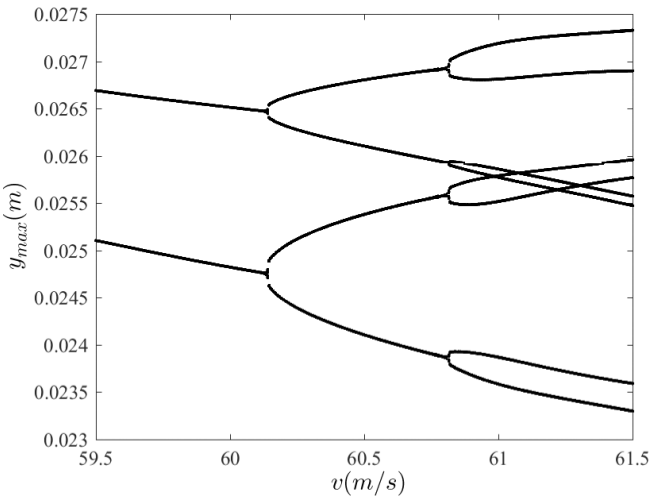

Fig. 14. A blow-up bifurcation diagram in the range 59.5–61.5 m/s.

increase of the speed). To give a clear description of the transitions we divide it into four regions as shown in Fig. 17. As the transitions in these four regions are similar, we only give a detailed description of region 1. Four-band chaos develops after the period doubling cascade. Two pairs of asymmetric chaotic attractors merge into two asymmetric chaotic attractors with the increase of the speed followed by another asymmetry breaking of the chaotic attractors, where only one chaotic attractor exists. When the speed reaches $V = 61.9684$ m/s a period-3 solution bifurcates from the chaotic attractor through a crisis followed by a period doubling cascade again, which leads the system into a broad-band chaos. Another crisis happens around $V = 62.1473$ m/s where the system jumps from the chaotic attractor to a limit cycle.

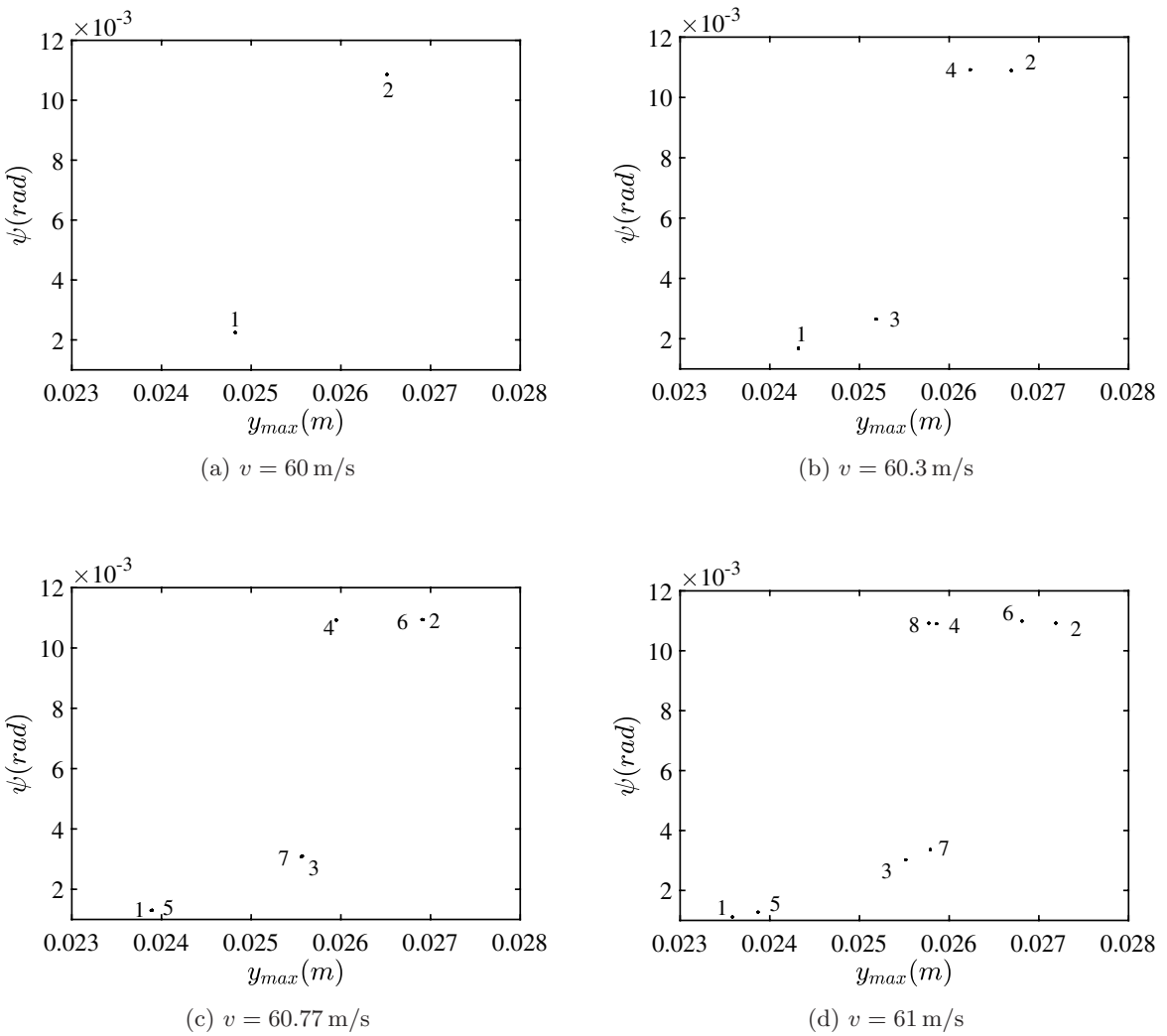

(a) $v = 60$ m/s

(b) $v = 60.3$ m/s

(c) $v = 60.77$ m/s

(d) $v = 61$ m/s

Fig. 15. Poincaré maps.

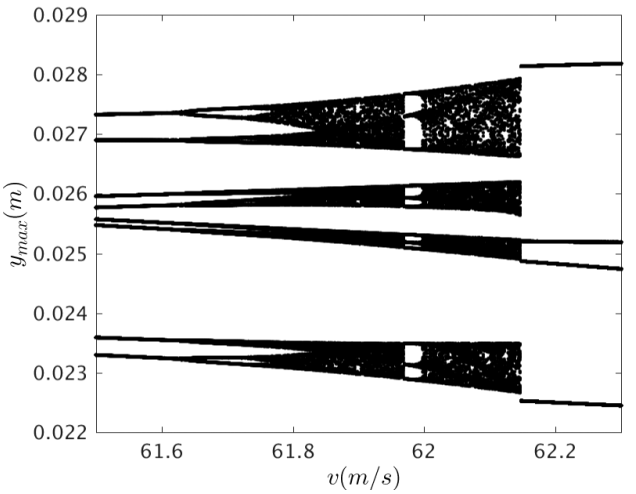

Fig. 16. A blow-up bifurcation diagram in the range 61.6–62.2 m/s.

From Fig. 16 it is seen that this system possesses hysteresis phenomenon in this speed range. We construct the bifurcation diagram again by decreasing the speed, which is shown in Fig. 18. It can be seen that another jump happens at around $V = 61.878$ m/s with the decrease of the speed, where a period-4 attractor jumps to the four-band chaotic attractor that can be recognized in Fig. 18.

4.4. *Speed range 62.5–65 m/s*

A blow-up bifurcation diagram in this speed range is shown in Fig. 19, which shows that the system alternates between periodic windows and chaotic attractors. At around $V = 62.7125$ m/s, the stable period-4 limit cycle loses stability through a crisis to two asymmetric chaotic attractors, which is

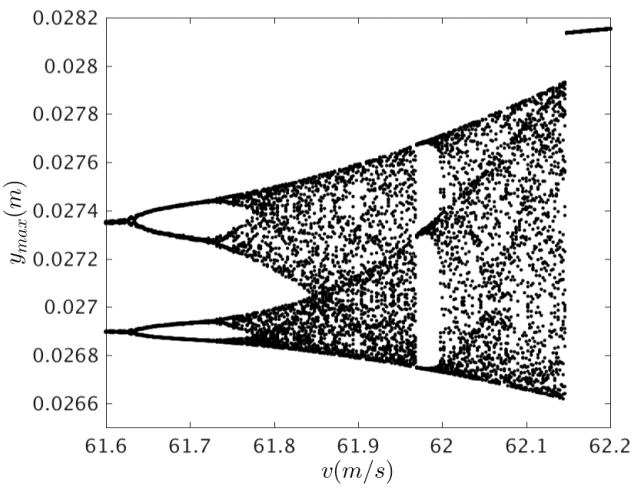

(a) Region 1

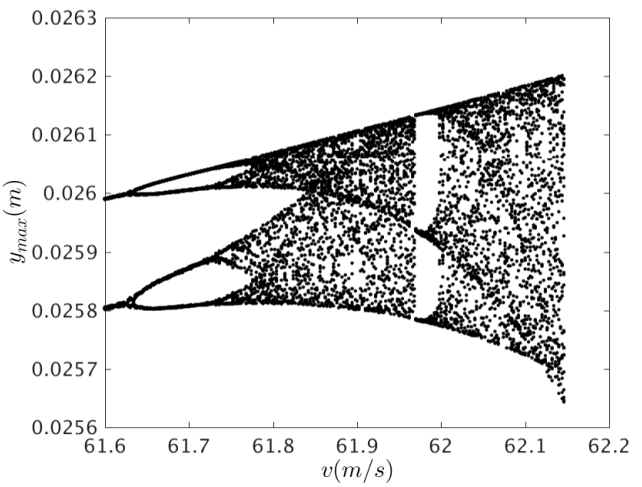

(b) Region 2

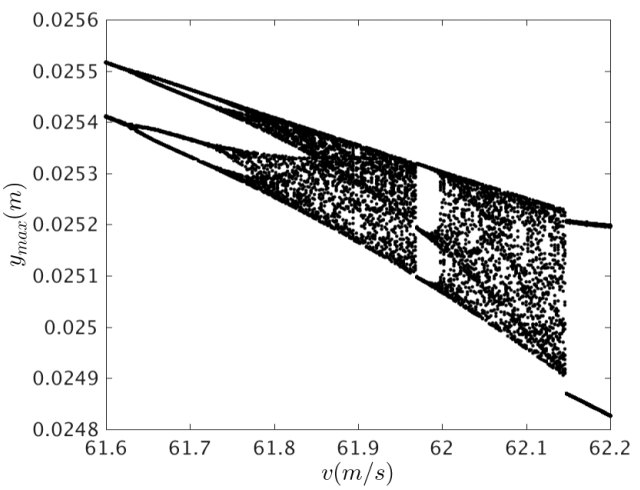

(c) Region 3

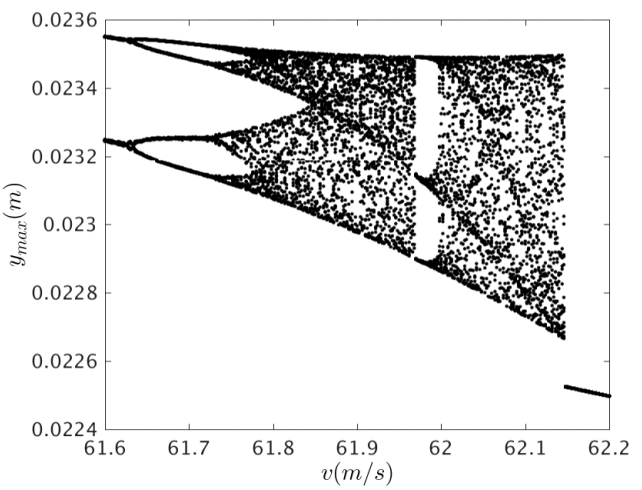

(d) Region 4

Fig. 17. Refined bifurcation diagrams of Fig. 16.

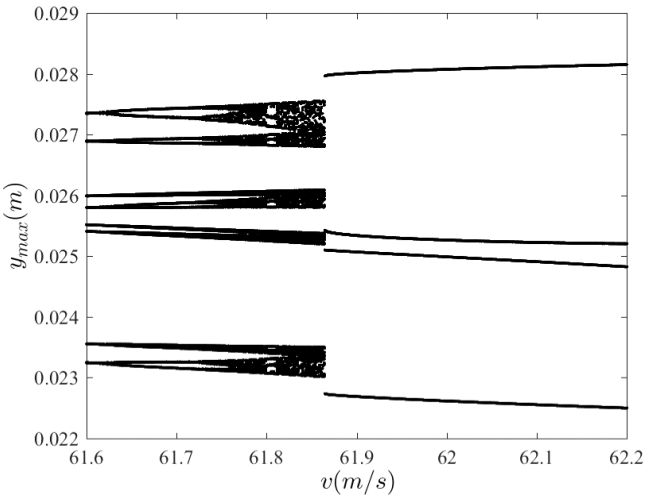

Fig. 18. Bifurcation diagram in the range 61.6–62.2 m/s by decreasing the speed.

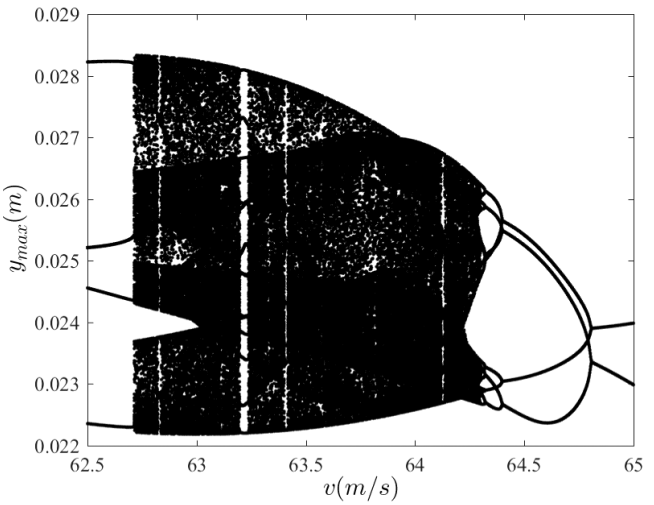

Fig. 19. A blow-up bifurcation diagram in the range 62.5–65 m/s.

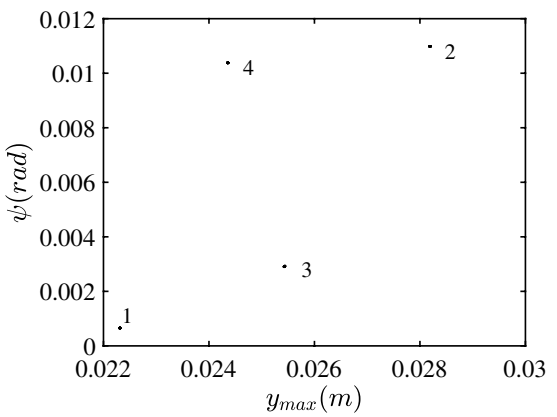

(a) $v = 62.7124$ m/s

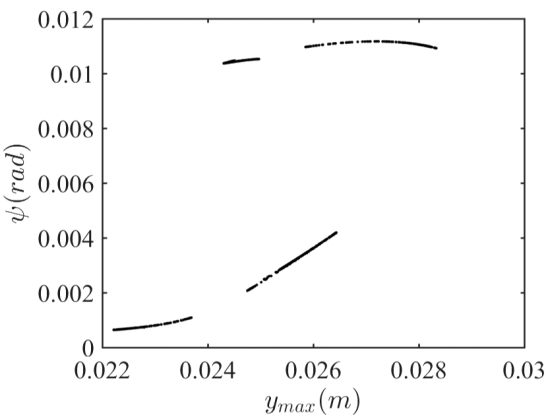

(b) $v = 62.7125$ m/s

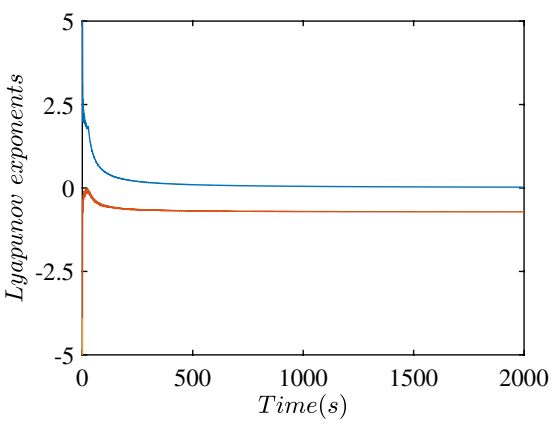

(c) $v = 62.7124$ m/s

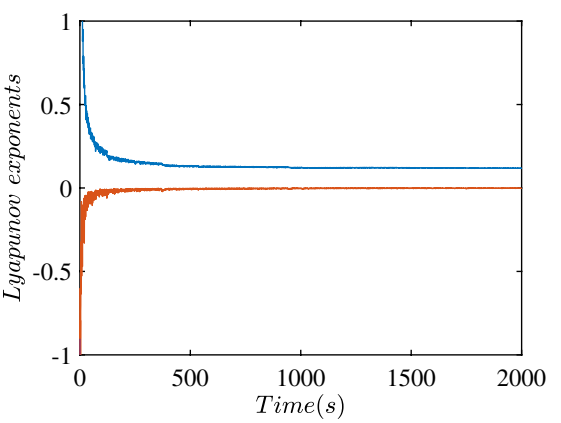

(d) $v = 62.7125$ m/s

Fig. 20. (a) and (b) Poincaré maps and (c) and (d) the two largest Lyapunov exponents of the system near the first crisis.

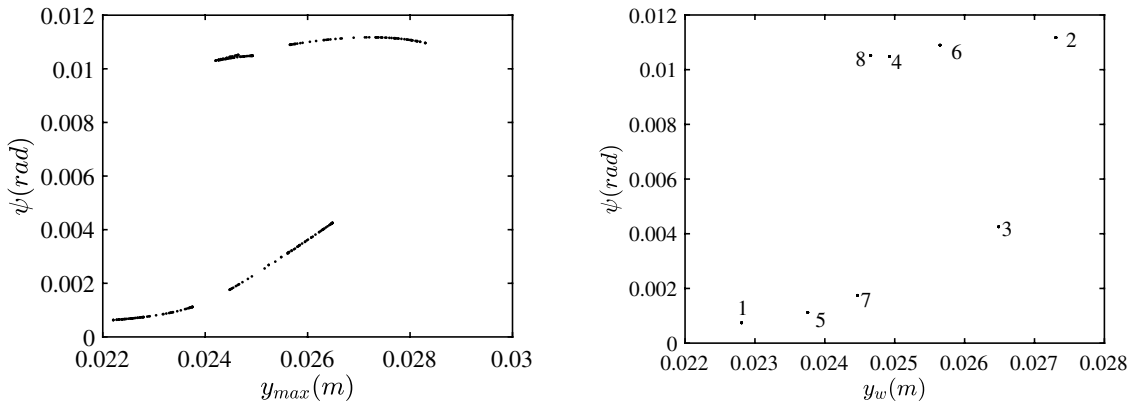

(a) $v = 62.8210\,\mathrm{m/s}$ (b) $v = 62.8212\,\mathrm{m/s}$

Fig. 21. Poincaré maps near the second crisis.

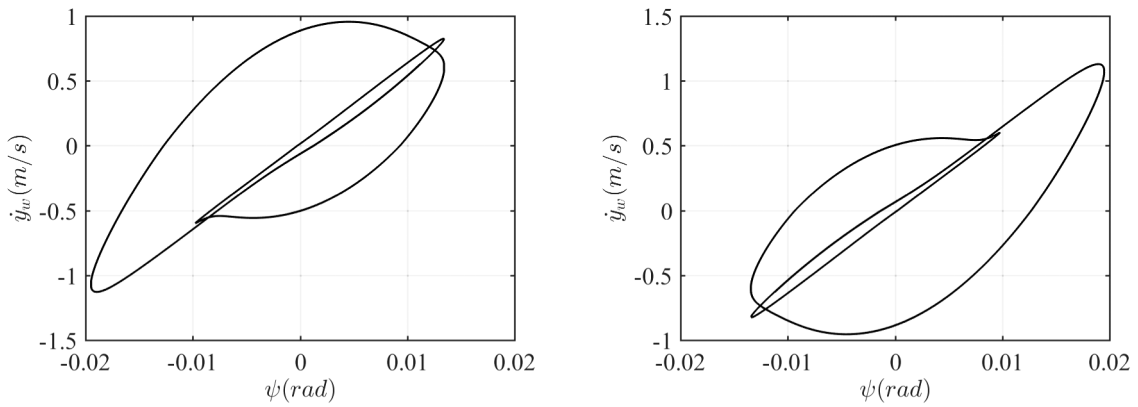

(a) Initial value 1 (b) Initial value 2

Fig. 22. Phase portraits of the model at $V = 65\,\mathrm{m/s}$.

confirmed by the Poincaré maps and the largest two Lyapunov exponents displayed in Fig. 20. The four points in Fig. 20(a) indicate a period-4 solution, and the stripes in Fig. 20(b) indicate chaos. These are confirmed by the two largest Lyapunov exponents of the system shown in Figs. 20(c) and 20(d), where the largest Lyapunov exponent changes from zero to a positive value. When the speed increases to $V = 62.8212\,\mathrm{m/s}$ the two asymmetric chaotic attractors lose stability through another crisis to a period-8 attractor, which is illustrated in Fig. 21 by the Poincaré maps similar to Fig. 20 but in a reserve transition. After a small range of periodic windows the asymmetric chaotic attractors regain stability. At still higher speed around $V = 63.0100\,\mathrm{m/s}$ the asymmetric chaotic attractors merge into a chaotic attractor. With the increase of the speed the chaotic attractor loses stability into a period 13 attractor. After several times of alternating between periodic windows and symmetric chaos, the system enters into asymmetric chaotic motions followed by a reverse period doubling cascade into two asymmetric limit cycles, which can be seen from the phase portrait of the system at $V = 65\,\mathrm{m/s}$ shown in Fig. 22 under two different initial values ($[x_1, x_2, x_3, x_4] = [0.0167\,\mathrm{m},\ 0.6299\,\mathrm{m/s},\ 0.0112\,\mathrm{rad},\ -0.2821\,\mathrm{rad/s}]$ and $[x_1, x_2, x_3, x_4] = [-0.0167\,\mathrm{m}, -0.6299\,\mathrm{m/s}, -0.0112\,\mathrm{rad}, 0.2821\,\mathrm{rad/s}]$) respectively.

5. Investigation of the Influence of the Conicity

In this section, we investigate the influence of the conicity of the wheels on both the Hopf bifurcation point and the first Lyapunov coefficient, which is used to determine the bifurcation form of the system. From Fig. 23 we can see that the speed

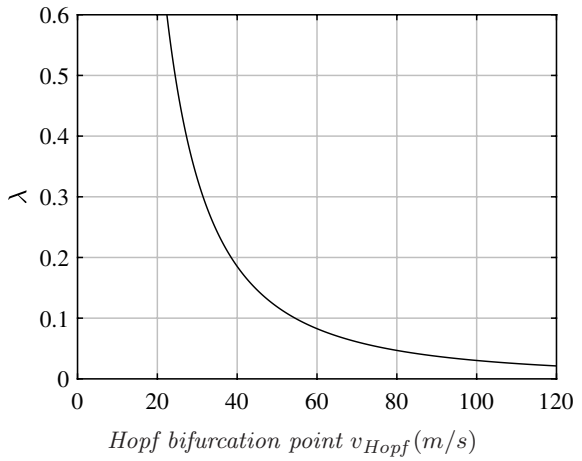

Fig. 23. Influence of the conicity on the Hopf bifurcation point.

corresponding to the Hopf bifurcation point, which is the linear critical speed of the wheelset system, decreases with the increase of the conicity. The value of the conicity has a significant influence on the Hopf bifurcation point when it is smaller than 0.1. Because of the wear of the wheels in the running process, the conicity of the wheels will change. Therefore, it is of interest to study the influence of the conicity on the bifurcation forms of the system. To have a clear knowledge of the influence of the conicity on the Hopf bifurcation forms of the system, the first Lyapunov coefficient of the system under different values of the conicity is calculated. From Fig. 24 we can see that when the conicity increases to 0.3420 the system changes from a subcritical Hopf bifurcation into a supercritical Hopf bifurcation. When the conicity reaches 0.4180, the first Lyapunov coefficient of the system changes sign from negative to positive, which means the system changes from a supercritical Hopf bifurcation into

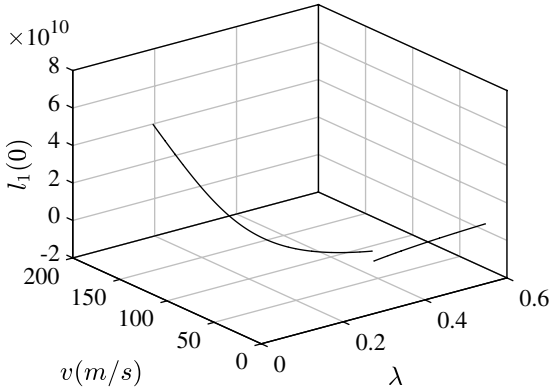

Fig. 24. Influence of the conicity on the first Lyapunov coefficient.

a subcritical Hopf bifurcation. It can be concluded that a subcritical Hopf bifurcation is common in the railway vehicle system in a wide range of the conicity.

6. Conclusion

In this paper, we investigate the lateral dynamics of a nonsmooth railway wheelset model, that consists of two degrees of freedom with linear characteristic springs and dry friction dampers. The nonlinear forces between the wheel and the rail are calculated by combining the linear kinematic relation between the wheel and the rail with nonlinear creepage-creep force relation [Vermeulen & Johnson, 1964]. This simple model has rich dynamical features. A variety of possible motions such as stable stationary motions, periodic motions, quasi-periodic motions and chaotic attractors are illustrated in this paper.

Unlike wheelset models with smooth dampers, the wheelset model with dry friction dampers has a set of stationary points under a low running speed. With the increase of the speed the stationary points lose stability through a subcritical Hopf bifurcation, where an unstable limit cycle bifurcates to the left side. The unstable limit cycle regains its stability through a fold bifurcation where a stable limit cycle bifurcates to the right side. A crossing-sliding bifurcation, which is special for nonsmooth dynamical systems, happens at $V = 44.5080\,\mathrm{m/s}$, where two sliding segments disappear.

At higher speed many complicated dynamical motions can happen. A Neimark–Sacker bifurcation occurs at $V = 56.2380\,\mathrm{m/s}$, where a two-dimensional torus develops. After several transitions between periodic and aperiodic motions, the two-dimensional torus loses its stability through a torus breakdown into a chaos followed by a crisis into two asymmetric periodic oscillations. Through a period doubling cascade the system enters into chaos again followed by another crisis around $V = 62.1473\,\mathrm{m/s}$, where the system enters into a period-4 oscillation. With a further increase of the speed, the motion of the system transits between chaos and periodic windows alternatively until a reverse period doubling casecade leads the system into two asymmetric limit cycles.

Since the conicity of the wheel, which will change with the wear of the wheel, is an important parameter for the lateral dynamics of the wheelset system, it is desirable to study the influence of this parameter value on the Hopf bifurcation point and

the bifurcation forms of the system. From the calculated results it can be seen that the conicity has a significant influence on the Hopf bifurcation point when it is lower than 0.1.

Acknowledgments

This work was supported by the China Railway Corporation under Grant No. 2016G008-A and Grant No. 2016J001-B and the Chinese Scholarship Council (CSC) Foundation.

References

Andronov, A. A., Khaikin, S. E. & Vitt, A. A. [1965] *Theory of Oscillators*, 1st edition (Pergamon Press, Oxford).

di Bernardo, M., Budd, C. J., Champneys, A. R. *et al.* [2008] *Piecewise-Smooth Dynamical Systems*: *Theory and Applications* (Springer-Verlag, London).

Carter, F. W. [1916] "The electric locomotive," *Minutes Proc. Instit. Civil Engin.* **201**, 221–252.

Eva, C. S. [1992] "Bifurkationer og kaos i en ikke-lineær model af et enkelt jernbanehjulsæt," PhD thesis, Technical University of Denmark.

Feigin, M. I. [1994] *Forced Oscillations in Systems with Discontinuous Nonlinearities* (Nauka, Moscow) (in Russian).

Filippov, A. F. [1988] *Differential Equations with Discontinuous Righthand Sides* (Kluwer Academic Publishers, Dortrecht).

Gao, X. J., Li, Y. H. & Yue, Y. [2012] "The 'resultant bifurcation diagram' method and its application to bifurcation behaviors of a symmetric railway bogie system," *Nonlin. Dyn.* **70**, 363–380.

Gao, X. J., Li, Y. H., Yue, Y. *et al.* [2013] "Symmetric/asymmetric bifurcation behaviours of a bogie system," *J. Sound. Vibr.* **332**, 936–951.

Gao, X. J., True, H. & Li, Y. H. [2015] "Lateral dynamic features of a railway vehicle," *Proc. IMechE Part F*: *J. Rail and Rapid Transit* **0**, 1–15.

Hoffmann, M. & Petersen, D. E. [2003] "Dry friction and impact dynamics in railway vehicles," Master thesis, Technical University of Denmark.

Huilgol, R. R. [1978] "Hopf-Friedrichs bifurcation and the hunting of a railway axle," *Quart. Appl. Math.* **36**, 85–94.

Jensen, C. N. & True, H. [1997] "On a new route to chaos in railway dynamics," *Nonlin. Dyn.* **13**, 117–129.

Kaas-Petersen, C. [1986a] "Chaos in a railway bogie," *Acta Mech.* **61**, 89–107.

Kaas-Petersen, C. [1986b] *PATH User's Guide* (Technical University of Denmark, Laboratory of Applied Mathematical Physics).

Klingel, J. [1883] "Über den Lauf der Eisenbahnwagen auf gerader Bahn. Organ für die Fortschritte des Eisenbahnwesens in technischer Beziehung," *Eisenbahnwesen Neue Folge.* **20**, 113–123.

Knudsen, C., Feldberg, R. & True, H. [1992] "Bifurcation and chaos in a model of a rolling railway wheelset," *Phil. Trans. Roy. Soc. Lond. A* **338**, 455–469.

Knudsen, C., Slivsgaard, E., Rose, M. *et al.* [1994] "Dynamics of a model of a railway wheelset," *Nonlin. Dyn.* **6**, 215–236.

Kuznetsov, Y. A. [2004] *Elements of Applied Bifurcation Theory*, 3rd edition (Springer-Verlag, NY).

Possel, R., Beautefoy, J. & Matsudaira, T. [1960] "Papers awarded prizes in the competition sponsored by Office of Research and Experiment (ORE) of the International Union of Railways (UIC)," ORE-Report RP2/SVA-C9, ORE, Utrecht.

Silvsgaard, E. & True, H. [1994] "Chaos in railway vehicle dynamics," *Nonlinearity and Chaos in Engineering Dynamics* (John Wiley & Sons, Chichester).

Simpson, D. J. W. [2010] *Bifurcations in Piecewise-Smooth Continuous Systems* (World Scientific, Singapore).

True, H. & Kaas-Petersen, C. [1983] "A bifurcation analysis of nonlinear oscillations in railway vehicles," *Veh. Syst. Dyn.* **12**, 5–6.

True, H. [1993] "On a new phenomenon in bifurcations of periodic orbits," *Dynamics*, *Bifurcation and Symmetry*, *New Trends and New Tools* (Springer, Netherlands), pp. 327–331.

True, H. & Asmund, R. [2002] "The dynamics of a railway freight wagon wheelset with dry friction damping," *Veh. Syst. Dyn.* **38**, 149–163.

True, H. & Thomsen, P. G. [2005] "On the problems of nonsmooth railway vehicle dynamics," *Proc. ECCOMAS Thematic Conf. Multibody Dynamics*, pp. 21–24.

True, H., Engsig-Karup, A. P. & Bigoni, D. [2013] "On the numerical and computational aspects of nonsmoothnesses that occur in railway vehicle dynamics," *Math. Comput. Simulat.* **95**, 78–97.

Vermeulen, P. J. & Johnson, K. L. [1964] "Contact of nonspherical elastic bodies transmitting tangential forces," *J. Appl. Mech.* **31**, 338–340.

Wolf, A., Swift, J. B., Swinney, H. L. *et al.* [1985] "Determining Lyapunov exponents from a time series," *Physica D* **16**, 285–317.

Xia, F. J. [2002] "The dynamics of the three-piece-freight truck," PhD thesis, Technical University of Denmark.

Zou, Y., Kupper, T. & Beyn, W. J. [2006] "Generalized Hopf bifurcation for planar Filippov systems continuous at the origin," *J. Nonlin. Sci.* **16**, 159–177.